Acoustic scaling of linear and mode-coupled anisotropic flow; implications for precision extraction of the specific shear viscosity

Peifeng Liu and Roy A. Lacey

Phys. Rev. C **98**, 021902 — Published 29 August 2018

DOI: 10.1103/PhysRevC.98.021902

Acoustic scaling of linear and mode-coupled anisotropic flow; implications for precision extraction of the specific shear viscosity

Peifeng Liu[1,2] and Roy A. Lacey[1,2,*]

[1] *Department of Chemistry, Stony Brook University, Stony Brook, NY, 11794-3400, USA*

[2] *Department of Physics and Astronomy, Stony Brook University, Stony Brook, NY, 11794-3800*

(Dated: April 16, 2018)

The $\mathrm{n^{th}}$-order linear flow coefficients $\mathrm{v_n^L}\,(\mathrm{n}=2,3,4,5)$, and the corresponding nonlinear mode-coupled (mc) coefficients $\mathrm{v^{mc}_{4,(2,2)}}$, $\mathrm{v^{mc}_{5,(2,3)}}$, $\mathrm{v^{mc}_{6,(3,3)}}$ and $\mathrm{v^{mc}_{6,(2,2,2)}}$, are studied for Pb+Pb collisions at $\sqrt{s_{\mathrm{NN}}} = 2.76$ TeV. Both sets of coefficients indicate a common acoustic scaling pattern of exponential viscous modulation, with a rate proportional to the square of the harmonic numbers and the mean transverse momenta (respectively), and inversely proportional to the cube root of the charged particle multiplicity $((\mathrm{N_{ch}})^{1/3})$, that characterizes the dimensionless size of the systems produced in the collisions. These patterns and their associated scaling parameters, provide new stringent constraints for eccentricity independent estimates of the specific shear viscosity $\frac{\eta}{s}(\mathrm{T})$ and the viscous correction to the thermal distribution function for the matter produced in the collisions. They also give crucial constraints for extraction of the initial-state eccentricity spectrum.

PACS numbers:

Anisotropic flow measurements play a crucial role in ongoing studies of the properties of the high energy-density quark-gluon plasma (QGP) created in relativistic heavy-ion collisions [1–8]. In particular, they provide an important avenue for the extraction of the specific shear viscosity (i.e., the ratio of shear viscosity to entropy density η/s) of the QGP, since they encode the viscous hydrodynamic response to the anisotropic transverse energy density profile produced in the early stages of the collision [3, 5–10].

In experiments, this flow manifests as an azimuthal asymmetry of the measured single-particle distribution and is routinely quantified by the complex flow vectors [9–11]:

$$\mathrm{V_n} \equiv \mathrm{v_n} e^{\mathrm{i}n\Psi_n} \equiv \{e^{\mathrm{i}n\phi}\}, \quad \mathrm{v_n} = \left\langle |\mathrm{V_n}|^2 \right\rangle^{1/2}, \qquad (1)$$

where ϕ denotes the azimuthal angle around the beam direction, of a particle emitted in the collision, $\{\dots\}$ denotes the average over all particles emitted in the event, and $\mathrm{v_n}$ and Ψ_n denote the magnitude and azimuthal direction of the $\mathrm{n^{th}}$-order harmonic flow vector which fluctuates from event to event. The coefficients $\mathrm{v_2}$ and $\mathrm{v_3}$ are commonly termed elliptic- and triangular flow respectively.

The initial anisotropic density profile $\rho_e(r,\varphi)$ (in the transverse plane) which drives anisotropic flow, can be similarly characterized by complex eccentricity coefficients [12–16]:

$$\mathcal{E}_\mathrm{n} \equiv \varepsilon_\mathrm{n} e^{\mathrm{i}n\Phi_n} \equiv -\frac{\int d^2\mathrm{r}_\perp\, \mathrm{r^m}\, e^{\mathrm{i}n\varphi}\, \rho_\mathrm{e}(\mathrm{r},\varphi)}{\int d^2\mathrm{r}_\perp\, \mathrm{r^m}\, \rho_\mathrm{e}(\mathrm{r},\varphi)}, \qquad (2)$$

where $\varepsilon_\mathrm{n} = \left\langle |\mathcal{E}_\mathrm{n}|^2 \right\rangle^{1/2}$ and Φ_n denote the magnitude and azimuthal direction of the $\mathrm{n^{th}}$-order eccentricity vector which also fluctuates from event to event; $\mathrm{m}=\mathrm{n}$ for $\mathrm{n}\geq 2$ and $\mathrm{m}=3$ for $\mathrm{n}=1$ [15, 17, 18].

Theoretical investigations show that $\mathrm{v_n} \propto \varepsilon_\mathrm{n}$ for elliptic- and triangular flow ($\mathrm{n} = 2$ and 3) [16, 19–21], albeit with a small anti-correlation between $\mathrm{v_2}$ and $\mathrm{v_3}$ [22, 23], which derives from an anti-correlation between ε_2 and ε_3 [24]; the latter is more important for peripheral collisions. Because the specific shear viscosity η/s, reduces the values of $\mathrm{v_n}$ and hence, the ratio $\mathrm{v_n}/\varepsilon_\mathrm{n}$, viscous hydrodynamical model comparisons to this ratio (implicit and explicit) have been employed to estimate both $\left\langle \frac{\eta}{s}(\mathrm{T}) \right\rangle$ and $\frac{\eta}{s}(\mathrm{T})$ [3, 5, 7, 8, 16, 25–30]. A recent state-of-the-art Bayesian multi-parameter analysis indicates a small value for $\left\langle \frac{\eta}{s}(\mathrm{T}) \right\rangle$ (i.e. 1-2 times the lower conjectured bound of $1/4\pi$ [31]), with substantial uncertainties of $\mathcal{O}(100\%)$, for both its magnitude and temperature dependence. Thus, there is still a pressing need to identify additional experimental constraints that can reduce existing bottlenecks for precision extraction of $\frac{\eta}{s}(\mathrm{T})$.

The higher order flow coefficients for $\mathrm{n} > 3$, reflect a linear response related to ε_n, as well as nonlinear mode-couplings derived from lower-order harmonics driven by eccentricities of the same harmonic order [10, 17, 18]:

$$\mathrm{V_4} = \mathrm{V_4^L} + \chi^{\mathrm{mc}}_{4,(2,2)}(\mathrm{V_2})^2, \qquad (3)$$

$$\mathrm{V_5} = \mathrm{V_5^L} + \chi^{\mathrm{mc}}_{5,(2,3)}\mathrm{V_2}\,\mathrm{V_3}, \qquad (4)$$

$$\mathrm{V_6} = \mathrm{V_6^L} + \chi^{\mathrm{mc}}_{6,(2,2,2)}(\mathrm{V_2})^3 + \chi^{\mathrm{mc}}_{6,(3,3)}(\mathrm{V_3})^2, \qquad (5)$$

$$\mathrm{V_7} = \mathrm{V_7^L} + \chi^{\mathrm{mc}}_{7,(2,2,3)}(\mathrm{V_2})^2\mathrm{V_3}, \qquad (6)$$

where $\chi^{\mathrm{mc}}_{\mathrm{n,(i,j)}}$ and $\chi^{\mathrm{mc}}_{\mathrm{n,(i,i,j)}}$ $(\mathrm{i}=2,\ \mathrm{j}=2,3)$ are $\mathrm{n^{th}}$-order nonlinear mode-coupling coefficients. In Eqs. 5 and 6 the nonlinear contributions are restricted to the two largest flow coefficients, $\mathrm{V_2}$ and $\mathrm{V_3}$ [10, 18].

If the linear and non-linear terms in Eqs. 3 - 6 are uncorrelated, the mode-coupling coefficients can be expressed as [10, 18]:

$$\chi^{\rm mc}_{4,(2,2)} = \frac{{\rm Re}\langle V_4 (V_2^*)^2\rangle}{\langle v_2^4\rangle}, \quad \chi^{\rm mc}_{5,(2,3)} = \frac{{\rm Re}\langle V_5 V_2^* V_3^*\rangle}{\langle v_2^2 v_3^2\rangle},$$
$$\chi^{\rm mc}_{6,(3,3)} = \frac{{\rm Re}\langle V_6 (V_3^*)^2\rangle}{\langle v_3^4\rangle}, \quad \chi^{\rm mc}_{6,(2,2,2)} = \frac{{\rm Re}\langle V_6 (V_2^*)^3\rangle}{\langle v_2^6\rangle},$$
$$\chi^{\rm mc}_{7,(2,2,3)} = \frac{{\rm Re}\langle V_7 (V_2^*)^2 V_3^*\rangle}{\langle v_2^4 v_3^2\rangle}. \quad (7)$$

For a given $\rm p_T$ and centrality selection, the magnitudes of the mode-coupled flow vectors can also be expressed in terms of the correlations of $\rm V_n$ with Ψ_2 and Ψ_3 to give [18, 32]:

$$\rm v^{mc}_{4,(2,2)} = \frac{\langle v_4 v_2^2 \cos(4\Psi_4 - 4\Psi_2)\rangle}{\sqrt{\langle v_2^4\rangle}} \approx \langle v_4 \cos(4\Psi_4 - 4\Psi_2)\rangle,$$
$$\rm v^{mc}_{5,(3,2)} = \frac{\langle v_5 v_3 v_2 \cos(5\Psi_5 - 3\Psi_3 - 2\Psi_2)\rangle}{\sqrt{\langle v_3^2\, v_2^2\rangle}}$$
$$\rm \approx \langle v_5\, \cos(5\Psi_5 - 3\Psi_3 - 2\Psi_2)\rangle,$$
$$\rm v^{mc}_{6,(2,2,2)} = \frac{\langle v_6\, v_2^3\, \cos(6\Psi_6 - 6\Psi_2)\rangle}{\sqrt{\langle v_2^6\rangle}} \approx \langle v_6 \cos(6\Psi_6 - 6\Psi_2)\rangle,$$
$$\rm v^{mc}_{6,(3,3)} = \frac{\langle \mathit{v}_6 \mathit{v}_3^2 \cos(6\Psi_6 - 6\Psi_3)\rangle}{\sqrt{\langle \mathit{v}_3^4\rangle}} \approx \langle v_6 \cos(6\Psi_6 - 6\Psi_3)\rangle,$$

where the average in the numerator is an average over particles for a given $\rm p_T$ selection, for all the events in the chosen centrality range, and the average in the denominator is an average over events for the centrality selection. These expressions point to the important role of event-plane correlations for mode-coupling. It is also straight forward to use Eqs. 3 - 7 to evaluate the magnitude of the higher-order linear harmonic response:

$$\rm v_4^L = \sqrt{v_4^2 - v_{4,(2,2)}^2}, \quad v_5^L = \sqrt{v_5^2 - v_{5,(3,2)}^2}. \quad (8)$$

Analogous to anisotropic flow, the complex eccentricity coefficients defined in Eq. 2, can be used to determine the higher-order mixed-mode eccentricities:

$$\varepsilon_{\rm n} = \sqrt{\left\langle |\mathcal{E}_n|^2\right\rangle}, \quad \varepsilon^{\rm mc}_{4,(2,2)} = \sqrt{\langle \epsilon_2^4\rangle},$$
$$\varepsilon^{\rm mc}_{5,(2,3)} = \sqrt{\langle \epsilon_2^2 \epsilon_3^2\rangle}, \quad \varepsilon^{\rm mc}_{6,(3,3)} = \sqrt{\langle \epsilon_3^4\rangle},$$
$$\varepsilon^{\rm mc}_{6,(2,2,2)} = \sqrt{\langle \epsilon_2^6\rangle}, \quad \varepsilon^{\rm mc}_{7,(2,2,3)} = \sqrt{\langle \epsilon_2^4 \epsilon_3^2\rangle}. \quad (9)$$

It has been argued that the linear response contribution to higher-order flow, should be linearly proportional to the cumulant-defined eccentricities $\mathcal{E}'_{\rm n}$ instead of $\mathcal{E}_{\rm n}$ [10]:

$$\mathcal{E}'_2 \equiv \epsilon_2 e^{i2\Phi_2} = \mathcal{E}_2, \qquad \mathcal{E}'_3 \equiv \epsilon_3 e^{i3\Phi_3} = \mathcal{E}_3,$$
$$\mathcal{E}'_4 \equiv \epsilon'_4 e^{i4\Phi'_4} \equiv -\frac{\langle z^4\rangle - 3\langle z^2\rangle^2}{\langle r^4\rangle} = \mathcal{E}_4 + \frac{3\langle r^2\rangle^2}{\langle r^4\rangle}\mathcal{E}_2^2,$$
$$\mathcal{E}'_5 \equiv \epsilon'_5 e^{i5\Phi'_5} \equiv -\frac{\langle z^5\rangle - 10\langle z^2\rangle\langle z^3\rangle}{\langle r^5\rangle} = \mathcal{E}_5 + \frac{10\langle r^2\rangle\langle r^3\rangle}{\langle r^5\rangle}\mathcal{E}_2\mathcal{E}_3, \quad (10)$$

where $z \equiv x + iy = re^{i\phi}$. An important advantage of this definition, is that it allows the subtraction of contributions from lower order z correlations.

In analogy to elliptic and triangular flow, $\rm v_n^L \propto \varepsilon_n^{'}$, $\rm v^{mc}_{n,(i,j)} \propto \varepsilon^{mc}_{n,(i,j)}$ and $\rm v^{mc}_{n,(i,i,j)} \propto \varepsilon^{mc}_{n,(i,i,j)}$. The specific shear viscosity also attenuates $\rm v_n^L/\varepsilon_n^{'}$, $\rm v^{mc}_{n,(i,j)}/\varepsilon^{mc}_{n,(i,j)}$ and $\rm v^{mc}_{n,(i,i,j)}/\varepsilon^{mc}_{n,(i,i,j)}$. For measurements at a given mean transverse momentum $\rm \langle p_T\rangle$, and centrality cent, this viscous attenuation can be expressed via an acoustic ansatz [24, 33–35] as:

$$\rm \frac{v_n^L}{\varepsilon_n^{'}} \propto \exp\left(-n^2\beta\frac{1}{RT}\right), \quad (11)$$
$$\rm \frac{v^{mc}_{n,(i,j)}}{\varepsilon^{mc}_{n,(i,j)}} \propto \exp\left(-(i^2+j^2)\beta\frac{1}{RT}\right),$$
$$\rm \frac{v^{mc}_{n,(i,i,j)}}{\varepsilon^{mc}_{n,(i,i,j)}} \propto \exp\left(-(2i^2+j^2)\beta\frac{1}{RT}\right), \quad (12)$$

where $\beta \propto \eta/s$, T is the temperature and R characterizes the geometric size of the collision zone. For a given centrality selection, the dimensionless size $\rm RT \propto N_{ch}^{1/3}$, where $\rm N_{ch}$ is the mid-rapidity charged hadron multiplicity density [36]. The magnitude of $\rm \langle N_{ch}\rangle$ is observed to factorize into a contribution proportional to the number of quark participant pairs $\rm N_{qpp}$ and a contribution proportional to $\log\left(\sqrt{\rm s_{NN}}\right)$ [36];

$$\rm \langle N_{ch}\rangle = N_{qpp}[b_{AA} + m_{AA}\log(\sqrt{s_{NN}})]^3$$
$$\rm b_{AA} = 0.530 \pm 0.008 \quad m_{AA} = 0.258 \pm 0.004. \quad (13)$$

Thus, for a given $\sqrt{\rm s_{NN}}$, variations in the magnitude of $\rm \langle N_{ch}\rangle$ largely reflects a change in $\rm N_{qpp}$. Indeed, for the simplifying assumption that $\rm R \propto (N_{qpp})^{1/3}$, Fig. 5 of Ref. [36] shows that the ratio $\rm [\langle N_{ch}\rangle/(N_{qpp})]^{1/3}$ is independent of R. This gives a further indication that, for a fixed value of $\sqrt{\rm s_{NN}}$, variations in the magnitude of the $\rm RT \propto \langle N_{ch}\rangle^{1/3}$ are not accompanied by sizable temperature changes. In contrast, a $\sqrt{\rm s_{NN}}$-driven variation of RT for a fixed value of $\rm N_{qpp}$, would result in significant temperature changes.

Equations 11 and 12 suggest characteristic linear dependencies for $\rm \ln(v_n^L/\varepsilon_n^{'})$, $\rm \ln(v^{mc}_{n,(i,j)}/\varepsilon^{mc}_{n,(i,j)})$ and $\rm \ln(v^{mc}_{n,(i,i,j)}/\varepsilon^{mc}_{n,(i,i,j)})$ on $\rm \langle N_{ch}\rangle^{-1/3}$ (respectively), with slopes that reflect specific quadratic viscous attenuation prefactors for β; these combined features are termed acoustic scaling. The prefactors, reflected in the slopes of $\rm \ln(v_n^L/\varepsilon_n^{'})$ vs. $\rm (N_{ch})^{-1/3}$, are not only expected to increase as $\rm n^2$, but should be approximately 2-3 times larger than those for $\rm \ln(v^{mc}_{n,(i,j)}/\varepsilon^{mc}_{n,(i,j)})$ and $\rm \ln(v^{mc}_{n,(i,i,j)}/\varepsilon^{mc}_{n,(i,i,j)})$ vs. $\rm (N_{ch})^{-1/3}$ (respectively) since $\rm (i^2+j^2) < n^2$.

Independent estimates of β, involving very different eccentricities, can also be obtained from the linear and mode-coupled harmonics. For example, the

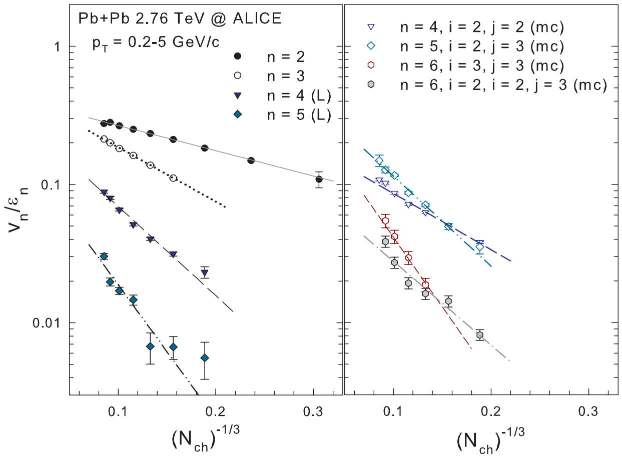

FIG. 1. Comparison of $(\mathrm{v_n^L}/\varepsilon_\mathrm{n}^{'})$ vs. $(\mathrm{N_{ch}})^{-1/3}$ for the linear harmonics (left panel), and $\mathrm{v^{mc}_{n,(i,j)}}/\varepsilon^{\mathrm{mc}}_{\mathrm{n,(i,j)}}$ and $\mathrm{v^{mc}_{n,(i,i,j)}}/\varepsilon^{\mathrm{mc}}_{\mathrm{n,(i,i,j)}}$ vs. $(\mathrm{N_{ch}})^{-1/3}$ (respectively) for the nonlinear mode-coupled harmonics, for Pb+Pb collisions at at $\sqrt{s_{NN}} = 2.76$ TeV. The lines represent a simultaneous exponential fit to the data, following Eqs. 11 and 12. The ALICE data are taken from Refs. [37, 38].

slope of the double ratio $\ln[(\mathrm{v^{mc}_{5,(2,3)}}/\varepsilon^{\mathrm{mc}}_{5,(2,3)})/(\mathrm{v}_2/\varepsilon_2)]$ vs. $(\mathrm{N_{ch}})^{-1/3}$, is expected to be similar to that for $\ln(\mathrm{v}_3/\varepsilon_3)$ vs. $(\mathrm{N_{ch}})^{-1/3}$ for a given $\langle \mathrm{p_T}\rangle$. Thus, the validation of simultaneous acoustic scaling of the linear and mode-coupled harmonics to give a single estimate of $\beta \propto \eta/s$, could provide a powerful constraint for initial-state eccentricity models and precision extraction of η/s.

In this letter, we use recent measurements of the linear and mode-coupled harmonics in Pb+Pb collisions at $\sqrt{s_{NN}} = 2.76$ TeV, to explore validation tests for simultaneous acoustic scaling of $\mathrm{v_n^L}/\varepsilon_\mathrm{n}^{'}$, $\mathrm{v^{mc}_{n,(i,j)}}/\varepsilon^{\mathrm{mc}}_{\mathrm{n,(i,j)}}$ and $\mathrm{v^{mc}_{n,(i,i,j)}}/\varepsilon^{\mathrm{mc}}_{\mathrm{n,(i,i,j)}}$, with an eye towards the development of new experimental constraints which could significantly reduce the large eccentricity-driven uncertainties associated with current extractions of η/s.

The data employed in this work are taken from the published flow measurements for Pb+Pb collisions at $\sqrt{s_{NN}} = 2.76$ TeV by the ALICE [37, 38] and ATLAS [22] collaborations. The ALICE centrality dependent $\mathrm{p_T}$-integrated measurements were performed for the harmonics $\mathrm{n} = 2, 3, 4, 5, 6$, for charged particles with pseudorapidity difference $|\Delta\eta| < 0.8$ and $0.2 < \mathrm{p_T} < 5.0$ GeV/c. Both the linear and mode-coupled flow coefficients were obtained directly via a two sub-events multiparticle correlation method. The corresponding ATLAS measurements were performed for $\mathrm{n} = 2, 3, 4, 5$ for particles with $2 < |\Delta\eta| < 5$ and for several $\mathrm{p_T}$ selections spanning the range $0.5 < \mathrm{p_T} < 4.0$ GeV/c, with the two-particle correlation method supplemented with event-shape selection [22]. The systematic uncertainties, which are included in our scaling analyses, are reported in Refs. [22, 37, 38] for both sets of measurements.

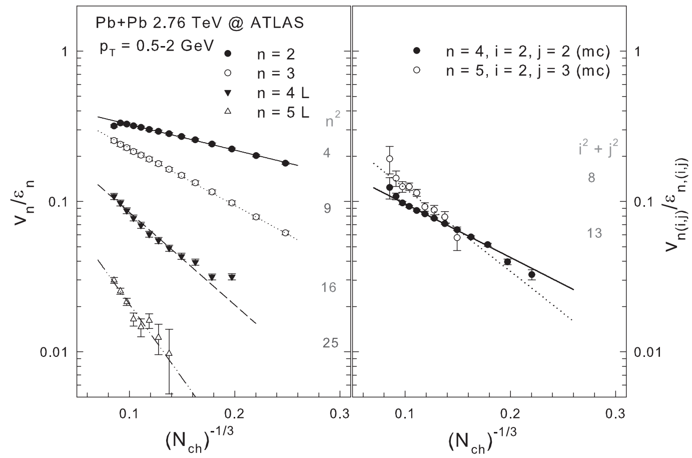

FIG. 2. Same as Fig. 1 but for ATLAS data [22]; the β-prefactors n^2 and $(\mathrm{i}^2 + \mathrm{j}^2)$ are indicated in the figure.

The requisite cumulant-defined eccentricities were calculated following the procedure outlined in Eqs. 2, 9 and 10 with the aid of a Monte Carlo quark-Glauber model (MC-qGlauber) with fluctuating initial conditions [39]. The model, which is based on the commonly used MC-Glauber model [40], was used to compute the number of quark participants $\mathrm{Nq_{part}}$(cent), and $\varepsilon_\mathrm{n}^{'}$(cent) and $\varepsilon^{\mathrm{mc}}_\mathrm{n}$(cent) from the two-dimensional profile of the density of sources in the transverse plane $\rho_s(\mathbf{r}_\perp)$ [10, 14, 39]. The model takes account of the finite size of the nucleon, the wounding profile of the nucleon, the distribution of quarks inside the nucleon and quark cross sections which reproduce the NN inelastic cross section at $\sqrt{s_{NN}} = 2.76$ TeV. A systematic uncertainty of 2-5% was estimated for the eccentricities from variations of the model parameters.

The centrality dependent multiplicity densities used to evaluate the dimensionless size $\mathrm{RT} \propto \mathrm{N_{ch}^{1/3}}$, are obtained from ALICE [41] and ATLAS [42] multiplicity density measurements. Validation tests for acoustic scaling were performed by plotting $\mathrm{v_n^L}/\varepsilon_\mathrm{n}^{'}$, $\mathrm{v^{mc}_{n,(i,j)}}/\varepsilon^{\mathrm{mc}}_{\mathrm{n,(i,j)}}$ and $\mathrm{v^{mc}_{n,(i,i,j)}}/\varepsilon^{\mathrm{mc}}_{\mathrm{n,(i,i,j)}}$ vs. $\langle\mathrm{N_{ch}}\rangle^{-1/3}$ respectively, to test for the expected patterns of exponential viscous attenuation, and the relative viscous attenuation β-prefactors indicated in Eqs. 11 and 12.

Figures 1 and 2 show the plots for $\mathrm{v_n^L}/\varepsilon_\mathrm{n}^{'}$, $\mathrm{v^{mc}_{n,(i,j)}}/\varepsilon^{\mathrm{mc}}_{\mathrm{n,(i,j)}}$ and $\mathrm{v^{mc}_{n,(i,i,j)}}/\varepsilon^{\mathrm{mc}}_{\mathrm{n,(i,i,j)}}$ vs. $(\mathrm{N_{ch}})^{-1/3}$ (respectively), for the ALICE (Fig. 1) and ATLAS (Fig. 2) data sets. They indicate the telltale acoustic scaling patterns of a characteristic linear dependence of $\ln(\mathrm{v_n^L}/\varepsilon_\mathrm{n}^{'})$, $\ln(\mathrm{v^{mc}_{n,(i,j)}}/\varepsilon^{\mathrm{mc}}_{\mathrm{n,(i,j)}})$ and $\ln(\mathrm{v^{mc}_{n,(i,i,j)}}/\varepsilon^{\mathrm{mc}}_{\mathrm{n,(i,i,j)}})$ on $(\mathrm{N_{ch}})^{-1/3}$ (respectively), with slope factors which strongly depend on the harmonic number n and the values of the mode-coupled harmonics i, j and i, i, j. Note that the slopes for the linear harmonics (left panel in each figure) show a much steeper dependence on $(\mathrm{N_{ch}})^{-1/3}$ than those for the mode-coupled

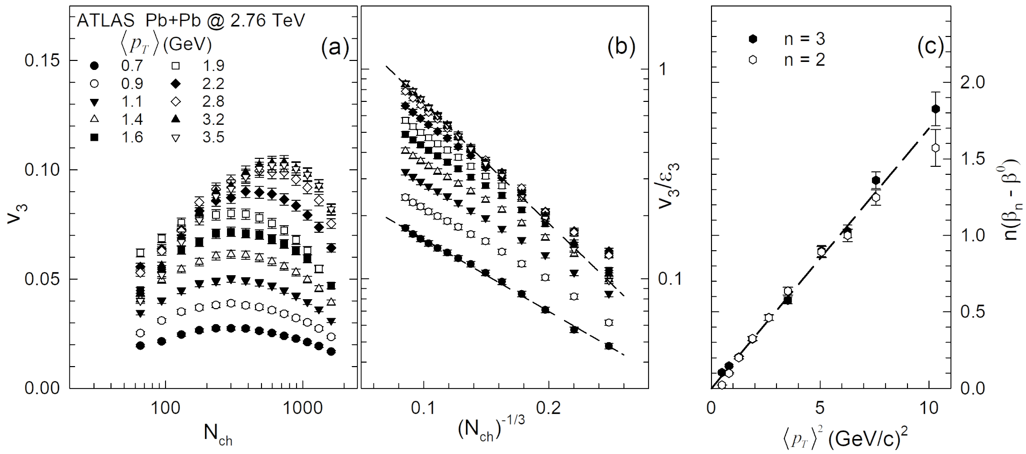

FIG. 3. (a) v_3 vs. N_{ch} for several $\langle p_T \rangle$ selections as indicated; (b) v_3/ε_3 vs. $(N_{ch})^{-1/3}$ for the data shown in (a). The dashed lines represent an exponential fit to the data for the selections $\langle p_T \rangle = 0.7$ and 3.5 GeV/c respectively. (c) $n(\beta_n - \beta^0)$ vs. $\langle p_T \rangle^2$ (see text); the slopes $n\beta_n$, are obtained from fits to the eccentricity-scaled data, similar to that shown in (b). The ATLAS data used in the plots are taken from Ref. [22]

harmonics (right panel in each figure), as expected from Eqs. 11 and 12. The expected slope hierarchy for both the linear and mode-coupled results are also apparent in both figures. The qualitative similarities between the results shown in Figs. 1 and 2 suggest that the respective methods employed by ATLAS and ALICE for extraction of the flow coefficients, are complementary.

The lines shown in Figs. 1 and 2 represent the results from fits to the data following Eqs. 11 and 12. They indicate that, within an uncertainty of $\sim 2-12\%$, a single slope value β, can account for the wealth of the linear and mode-coupled measurements in each data set. That is, they confirm the quadratic β prefactors of 4, 9, 16 and 25 for v_n^L (n=2,3,4 and 5) and 8, 13, 18 and 12 for $v^{mc}_{4,(2,2)}$, $v^{mc}_{5,(2,3)}$, $v^{mc}_{6,(3,3)}$ and $v^{mc}_{6,(2,2,2)}$ respectively. To estimate the fit uncertainty for each data set, the slope for the fit to v_2/ε_2 was first obtained, and then used in conjunction with the quadratic prefactors to quantify slope deviations from one.

The value of β also depend on p_T, even though this is not explicitly indicated in Eqs. 11 and 12. In hydrodynamical models, this p_T dependence can be understood in terms of the first viscous correction δf, to the thermal distribution function [43, 44]. It leads to an additional viscous attenuation factor $\propto p_T^{\alpha}$, where current theoretical estimates indicate the range 1-2 for α [43, 44]. That is, β is expected to increase as p_T^{α}, where the value of α is currently not fully constrained.

An experimental constraint for α can be obtained via acoustic scaling of the differential measurements $v_n(N_{ch})$, for different $\langle p_T \rangle$ selections as illustrated in Fig. 3. Panel (a) shows a steepened decrease of v_3 with $\langle p_T \rangle$, for $N_{ch} \lesssim 400$. This pattern results from an increase in the viscous attenuation with $\langle p_T \rangle$. This attenuation is made more transparent in Fig. 3(b), where (v_3/ε_3) vs. $(N_{ch})^{-1/3}$ is plotted for several $\langle p_T \rangle$ selections as indicated. The characteristic linear dependence of $\ln(v_3/\varepsilon_3)$ on $(N_{ch})^{-1/3}$ (i.e., exponential viscous attenuation), is clearly visible for each $\langle p_T \rangle$ selection. It is also apparent that the slopes β, for $\ln(v_3/\varepsilon_3)$ vs. $(N_{ch})^{-1/3}$ increases with $\langle p_T \rangle$ over the range indicated. This increase reflects the additional viscous attenuation factor due to δf.

The slopes, obtained from fits to (v_3/ε_3) vs. $(N_{ch})^{-1/3}$ (c.f. panel (b)) and (v_2/ε_2) vs. $(N_{ch})^{-1/3}$, for each $\langle p_T \rangle$ selection, are plotted vs. $\langle p_T \rangle^2$ in panel (c). Note that the plotted slopes are $\beta_n^{\delta f} \equiv n(\beta_n - \beta^0)$, where $\beta^0 = 0.83 \pm 0.04$, is the value for $p_T = 0.0$ GeV/c. The dashed line, which shows a linear fit to the data, indicates that $\beta_n^{\delta f}$ increases as $\langle p_T \rangle^2$, i.e., $\beta_n^{\delta f} = nkp_T^2$ where $k = 0.169 \pm 0.003\,\mathrm{GeV}^{-2}$ for these data. These results provide a clear constraint for α and $\beta_n^{\delta f}$, and consequently, the first viscous correction to the thermal distribution function in viscous hydrodynamical models.

The scaling patterns shown in Fig. 3(c) indicate that the viscous coefficient in Eq. 11 can be expressed as $n^2\beta = n(n\beta^0 + kp_T^2)$ and used to extract β^0 from ratios of the eccentricity scaled harmonics. Fig. 4(a) shows the β^0 values extracted from $\ln[(v_3/\varepsilon_3)/(v_2/\varepsilon_2)]$ vs. $(N_{ch})^{-1/3}$ for several values of $\langle p_T \rangle$; the prefactors are 5 $(n^2 - m^2)$ and 1 $(n - m)$ for β^0 and $\beta^{\delta f}_{n-m}$, respectively. Fig. 4(a) indicates that the extracted β^0 values are essentially p_T-independent over the $\langle p_T \rangle$ range of interest. This p_T-independence confirms that the pattern of viscous attenuation, due to δf, is similar for v_n and v_m with magnitudes that differ by the value $(n - m)kp_T^2$. Fig. 4(b) shows that similar magnitudes and trends are obtained for the empirical ratio $(v_2/\varepsilon_2)^{1/2}/(v_3/\varepsilon_3)^{1/3}$ vs. $\langle p_T \rangle^2$ [33], indicating that the δf-driven viscous attenuation factor nkp_T^2, cancels for this ratio. Thus, the ratio $(v_n/\varepsilon_n^{'})^{1/n}/(v_2/\varepsilon_2)^{1/2}$ vs. $\langle p_T \rangle^2$ can be used to further

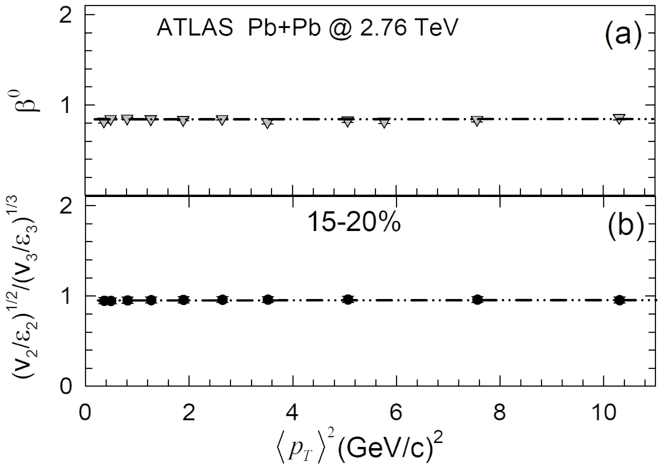

FIG. 4. (a) β^0 vs. $\langle \mathrm{p_T}\rangle^2$; the β^0 values are extracted from plots of $\ln[(\mathrm{v}_3/\varepsilon_3)/(\mathrm{v}_2/\varepsilon_2)]$ vs. $(\mathrm{N_{ch}})^{-1/3}$, for several $\langle \mathrm{p_T}\rangle$ selections (see text). (b) $(v_2/\varepsilon_2)^{1/2}/(v_3/\varepsilon_3)^{1/3}$ vs. $\langle \mathrm{p_T}\rangle^2$ for 15-20% central Pb+Pb collisions. The dashed lines in both panels are drawn to guide the eye. The ATLAS data used in the plots are taken from Ref. [22]

constrain β^0 and the eccentricity spectrum.

The present analysis shows that an eccentricity- and $\mathrm{p_T}$-independent estimate of $\beta^0 \propto \left\langle \frac{\eta}{s}(\mathrm{T})\right\rangle$ can be constrained by simultaneous acoustic scaling of both the linear and mode-coupled differential flow coefficients. However, a further calibration would be required to map β^0 on to the the actual value of $\left\langle \frac{\eta}{s}(\mathrm{T})\right\rangle$ for the QGP. An appropriately constrained set of viscous hydrodynamical calculations, tuned to reproduce the results shown in Figs. 1 - 4, could provide such a calibration to give a relatively precise estimate of $\left\langle \frac{\eta}{s}(\mathrm{T})\right\rangle$, as well as simultaneous verification of the initial-state eccentricity spectrum. Further studies for different beam energies, could provide additional stringent constraints for $\frac{\eta}{s}(\mathrm{T})$

In summary, we have presented a detailed phenomenological investigation for new constraints designed to facilitate precision extraction of η/s. We find that the linear flow coefficients $\mathrm{v_n^L}$ $(\mathrm{n} = 2, 3, 4, 5)$, and the nonlinear mode-coupled coefficients $\mathrm{v^{mc}_{4,(2,2)}}$, $\mathrm{v^{mc}_{5,(2,3)}}$, $\mathrm{v^{mc}_{6,(3,3)}}$ and $\mathrm{v^{mc}_{6,(2,2,2)}}$, follow a common acoustic scaling pattern of exponential viscous modulation in the created medium, at a rate proportional to the square of the harmonic numbers, and inversely proportional to the dimensionless size $\mathrm{RT} \propto (\mathrm{N_{ch}})^{1/3}$. The scaling patterns of specific ratios of the eccentricity scaled harmonics, also indicate a characteristic square dependence on particle transverse momenta. These patterns and their associated scaling parameters, could provide stringent new constraints for eccentricity independent estimates of $\left\langle \frac{\eta}{s}(\mathrm{T})\right\rangle$ and the first viscous correction to the thermal distribution function, as well as the initial-state eccentricity spectrum.

Acknowledgments This research is supported by the US DOE under contract DE-FG02-87ER40331.A008.

---

* E-mail: Roy.Lacey@Stonybrook.edu

[1] D. Teaney, Phys.Rev. **C68**, 034913 (2003), arXiv:nucl-th/0301099 [nucl-th].
[2] R. A. Lacey and A. Taranenko, PoS **CFRNC2006**, 021 (2006), arXiv:nucl-ex/0610029 [nucl-ex].
[3] P. Romatschke and U. Romatschke, Phys.Rev.Lett. **99**, 172301 (2007), arXiv:0706.1522 [nucl-th].
[4] M. Luzum and P. Romatschke, Phys.Rev. **C78**, 034915 (2008), arXiv:0804.4015 [nucl-th].
[5] H. Song, S. A. Bass, U. Heinz, T. Hirano, and C. Shen, Phys. Rev. Lett. **106**, 192301 (2011), [Erratum: Phys. Rev. Lett.109,139904(2012)], arXiv:1011.2783 [nucl-th].
[6] J. Qian, U. W. Heinz, and J. Liu, Phys. Rev. **C93**, 064901 (2016), arXiv:1602.02813 [nucl-th].
[7] B. Schenke, S. Jeon, and C. Gale, Phys.Lett. **B702**, 59 (2011), arXiv:1102.0575 [hep-ph].
[8] F. G. Gardim, F. Grassi, M. Luzum, and J.-Y. Ollitrault, Phys.Rev.Lett. **109**, 202302 (2012), arXiv:1203.2882 [nucl-th].
[9] M. Luzum, J. Phys. **G38**, 124026 (2011), arXiv:1107.0592 [nucl-th].
[10] D. Teaney and L. Yan, Phys. Rev. **C86**, 044908 (2012), arXiv:1206.1905 [nucl-th].
[11] J.-Y. Ollitrault, Phys. Rev. **D46**, 229 (1992).
[12] B. H. Alver, C. Gombeaud, M. Luzum, and J.-Y. Ollitrault, Phys. Rev. **C82**, 034913 (2010), arXiv:1007.5469 [nucl-th].
[13] H. Petersen, G.-Y. Qin, S. A. Bass, and B. Muller, Phys. Rev. **C82**, 041901 (2010), arXiv:1008.0625 [nucl-th].
[14] R. A. Lacey, R. Wei, N. N. Ajitanand, and A. Taranenko, Phys. Rev. **C83**, 044902 (2011), arXiv:1009.5230 [nucl-ex].
[15] D. Teaney and L. Yan, Phys. Rev. **C83**, 064904 (2011), arXiv:1010.1876 [nucl-th].
[16] Z. Qiu and U. W. Heinz, Phys. Rev. **C84**, 024911 (2011), arXiv:1104.0650 [nucl-th].
[17] R. S. Bhalerao, J.-Y. Ollitrault, and S. Pal, Phys. Lett. **B742**, 94 (2015), arXiv:1411.5160 [nucl-th].
[18] L. Yan and J.-Y. Ollitrault, Phys. Lett. **B744**, 82 (2015), arXiv:1502.02502 [nucl-th].
[19] J. Fu, Phys. Rev. **C92**, 024904 (2015).
[20] H. Niemi, K. J. Eskola, and R. Paatelainen, Phys. Rev. **C93**, 024907 (2016), arXiv:1505.02677 [hep-ph].
[21] J. Noronha-Hostler, L. Yan, F. G. Gardim, and J.-Y. Ollitrault, Phys. Rev. **C93**, 014909 (2016), arXiv:1511.03896 [nucl-th].
[22] G. Aad et al. (ATLAS), Phys. Rev. **C92**, 034903 (2015), arXiv:1504.01289 [hep-ex].
[23] J. Adam et al. (ALICE), Phys. Rev. Lett. **117**, 182301 (2016), arXiv:1604.07663 [nucl-ex].
[24] R. A. Lacey, D. Reynolds, A. Taranenko, N. N. Ajitanand, J. M. Alexander, F.-H. Liu, Y. Gu, and A. Mwai, J. Phys. **G43**, 10LT01 (2016), arXiv:1311.1728 [nucl-ex].

[25] T. Hirano, U. W. Heinz, D. Kharzeev, R. Lacey, and Y. Nara, Phys.Lett. **B636**, 299 (2006), arXiv:nucl-th/0511046 [nucl-th].

[26] B. Schenke, S. Jeon, and C. Gale, Phys.Rev.Lett. **106**, 042301 (2011), arXiv:1009.3244 [hep-ph].

[27] P. Bozek, M. Chojnacki, W. Florkowski, and B. Tomasik, Phys.Lett. **B694**, 238 (2010), arXiv:1007.2294 [nucl-th].

[28] H. Niemi, G. Denicol, P. Huovinen, E. Molnar, and D. Rischke, Phys.Rev. **C86**, 014909 (2012), arXiv:1203.2452 [nucl-th].

[29] S. McDonald, C. Shen, F. Fillion-Gourdeau, S. Jeon, and C. Gale, Phys. Rev. **C95**, 064913 (2017), arXiv:1609.02958 [hep-ph].

[30] J. E. Bernhard, J. S. Moreland, S. A. Bass, J. Liu, and U. Heinz, (2016), arXiv:1605.03954 [nucl-th].

[31] P. Kovtun, D. Son, and A. Starinets, Phys.Rev.Lett. **94**, 111601 (2005), arXiv:hep-th/0405231 [hep-th].

[32] R. S. Bhalerao, J.-Y. Ollitrault, and S. Pal, Phys. Rev. **C88**, 024909 (2013), arXiv:1307.0980 [nucl-th].

[33] R. A. Lacey, A. Taranenko, N. Ajitanand, and J. Alexander, (2011), arXiv:1105.3782 [nucl-ex].

[34] R. A. Lacey, Y. Gu, X. Gong, D. Reynolds, N. Ajitanand, et al., (2013), arXiv:1301.0165 [nucl-ex].

[35] E. Shuryak and I. Zahed, (2013), arXiv:1301.4470 [hep-ph].

[36] R. A. Lacey, P. Liu, N. Magdy, M. Csand, B. Schweid, N. N. Ajitanand, J. Alexander, and R. Pak, (2016), arXiv:1601.06001 [nucl-ex].

[37] S. Acharya et al. (ALICE), Phys. Lett. **B773**, 68 (2017), arXiv:1705.04377 [nucl-ex].

[38] K. Aamodt et al. (ALICE Collaboration), Phys.Rev.Lett. **107**, 032301 (2011), arXiv:1105.3865 [nucl-ex].

[39] Pifeng Liu and Roy A. Lacey, to be published.

[40] M. L. Miller, K. Reygers, S. J. Sanders, and P. Steinberg, Ann. Rev. Nucl. Part. Sci. **57**, 205 (2007); B. Alver et al., Phys. Rev. Lett. **98**, 242302 (2007).

[41] K. Aamodt et al. (ALICE), Phys. Rev. Lett. **106**, 032301 (2011), arXiv:1012.1657 [nucl-ex].

[42] G. Aad et al. (ATLAS), Phys. Lett. **B710**, 363 (2012), arXiv:1108.6027 [hep-ex].

[43] K. Dusling, G. D. Moore, and D. Teaney, Phys.Rev. **C81**, 034907 (2010), arXiv:0909.0754 [nucl-th].

[44] D. A. Teaney, in Quark-gluon plasma 4, edited by R. C. Hwa and X.-N. Wang (2010) pp. 207–266, arXiv:0905.2433 [nucl-th].